Journal of Power Sources 198 (2012) 203–217

Contents lists available at SciVerse ScienceDirect

Journal of Power Sources

journal homepage: www.elsevier.com/locate/jpowsour

# Modeling of current mode controlled boost converter supplied by fuel cell suitable for controller design purposes

Toni Bjažić[a,*], Željko Ban[a], Miro Milanovič[b]

[a] University of Zagreb, Faculty of Electrical Engineering and Computing, Unska 3, 10000 Zagreb, Croatia
[b] University of Maribor, Faculty of Electrical Engineering and Computer Science, Smetanova 17, 2000 Maribor, Slovenia

ARTICLE INFO

*Article history:*
Received 27 June 2011
Received in revised form
21 September 2011
Accepted 25 September 2011
Available online 1 October 2011

*Keywords:*
Modeling
Linear model
Boost converter
Peak current mode control
PEM fuel cell

ABSTRACT

This paper presents the derivation of a linear model with changeable parameters of constant frequency peak current mode controlled DC/DC boost converter supplied by a PEM fuel cell stack. The derived model has the same structure irrespective of the conduction mode and therefore, it is suitable for design of simple and advanced controllers of the output voltage. Experimental results on the system with 450 W boost converter supplied by PEM fuel cell emulator show that the derived model accurately describes the system in a given operating point, determined by the load resistance or output current.



## 1. Introduction

Hydrogen is a promising energy source in the near future, since it can be transformed into electrical energy using fuel cells. All benefits of using hydrogen as possible replacement for fossil fuels are well known. Hydrogen is the cleanest, the lightest and the most efficient fuel. Since hydrogen is not a primary energy source, it must be generated from other energy sources (e.g. steam reformation of natural gas) or by using other energy sources for water electrolysis. Therefore, other sources of energy should be renewable (e.g. wind, sun, ...) to remain in the spirit of clean energy production.

There are numerous researches in which different systems topologies with fuel cells are presented [1–11]. All topologies have a DC/DC converter as the common part of the system, which stabilizes the DC voltage from the fuel cell at a certain (usually fixed) value.

Control of the fuel cell voltage is possible by controlling the airflow through the cathode side and the hydrogen pressure on the anode side of the fuel cell. Since the fuel cell is a nonlinear control system, some advanced control techniques should be used to obtain the desired transient behavior of the system and steady state accuracy. In [12] an indirect model reference adaptive control is used to control the fuel cell voltage, while in [13] the model reference adaptive control with signal adaptation algorithm is used for the same purpose. A time delay control is used in [14], to improve the fuel cell transient responses and at the same time to prevent flooding and air starvation. Some advanced nonlinear control techniques are suggested in [15–21]. Irrespective of the used advanced control system, the dynamics of such a system is rather slow (few seconds or even tens of seconds), due to the nature of the control valves and the hydrogen and airflow dynamics. On the other hand, the electrical part of the fuel cell has a fast dynamic response, which could not be efficiently controlled by input control valves. Therefore, it is inevitable to control the DC/DC converter's output voltage to achieve fast transient responses (milliseconds) and steady state accuracy.

This paper deals with the concept of DC/DC boost converter supplied by the fuel cell. The output voltage of the fuel cell BCS 64-32 [22] ranges from 19 V to 31 V and the boost converter has to raise it to 50 V.

The boost converter is a nonlinear and non-minimum phase system, and because of that, its control must be considered very carefully. There are two essential control techniques based on pulse width modulation (PWM): voltage mode control (VMC) and current mode control (CMC). In applications that require vary fast transient responses the current mode control is usually chosen. There are three main advantages of current mode control:

(i) faster response to the change of referent voltage due to the very fast current loop, which acts like a controllable current source,

* Corresponding author. Tel.: +385 16129529; fax: +385 16129809.
*E-mail addresses:* toni.bjazic@fer.hr (T. Bjažić), zeljko.ban@fer.hr (Ž. Ban), milanovic@uni-mb.si (M. Milanovič).

0378-7753/$ – see front matter © 2011 Elsevier B.V. All rights reserved.
doi:10.1016/j.jpowsour.2011.09.079

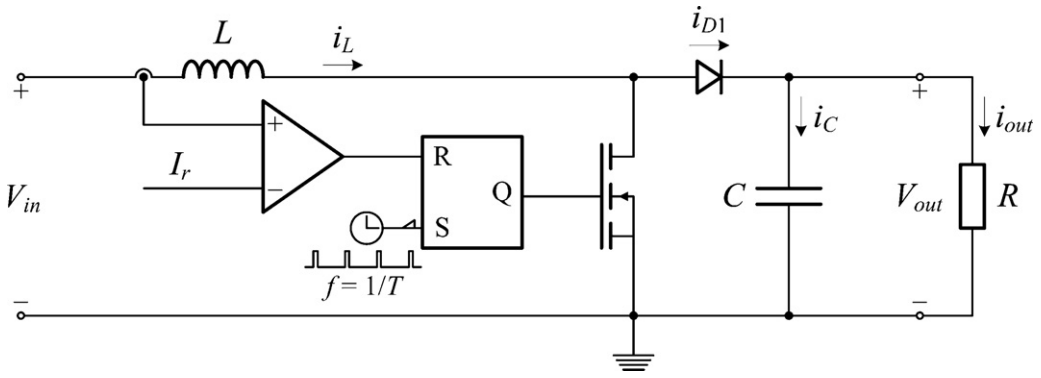


**Fig. 1.** The conceptual scheme of the DC/DC boost converter in peak current mode control.

(ii) the system order is reduced by one, which enables easier design of the outer control loop and
(iii) inherently fast overcurrent protection.

The main disadvantage of the current mode control is the well known instability for duty cycles greater than 0.5. This problem is easily solved by introducing a compensation ramp for constant frequency applications [23] or constant on/off times for variable frequency applications [24,25].

In both control modes the converter can operate in continuous or discontinuous conduction mode.

Modeling of the VMC converter in continuous conduction mode is easily done by using the well known averaging techniques [26,23]. In [27] an averaged modeling of converters operating in discontinuous conduction modes is described.

Modeling of CMC converters depends on the chosen technique of dealing with instability in duty cycles greater than 0.5. Literature dealing with constant frequency current mode control [23,28,29] usually concentrates on obtaining high accuracy dynamic models in continuous or discontinuous conduction modes. From the control point of view, this high accuracy for individual conduction modes (especially at high frequencies) is not so important as obtaining accurate steady-state gain and dominant time constant. Furthermore, transfer functions that are obtained for controller design are not directly applicable because they describe the behavior of the output voltage with respect to the change of duty cycle, rather than the referent (peak) current with included compensation ramp, as they should.

This paper focuses on obtaining a unique linear model with changeable parameters of the CMC boost converter, which is valid in continuous and discontinuous conduction modes and is suitable for the design of a voltage control loop. The model obtained is used in [30] to design an adaptive control system, able to achieve approximately the same dynamic behavior of the system, irrespective of the conduction mode and resistive load at its output.

The model of constant frequency peak current mode controlled DC/DC boost converter is described in Section 2. The fuel cell model is described in Section 3. The integrated process model is described in Section 4 and the experimental identification of control system parameters is carried out in Section 5. Finally, some conclusions are given in Section 6.

## 2. Modeling of peak current mode controlled DC/DC boost converter

The model of the converter applicable for the control purpose must describe the output voltage as a function of the referent current and input voltage. The model must have a linear form in the constant operating point with parameters of the model described as a function of the operating point values.

The conceptual scheme of the DC/DC boost converter in peak current mode control is shown in Fig. 1 [23]. Unlike the voltage mode control, the inductor current signal is used for modulation, which also has a sawtooth or triangular shape. The transistor is switched on at the beginning of each period by setting the bistable (S input), and switched off at the time when the inductor current reaches the referent current value $I_r$ (bistable R input).

The dynamic analysis of the peak current mode controlled boost converter is based on a method of injected and absorbed current [23]. According to the method, the inductor and the switching elements (comparator, bistable, transistor and diode) shown in Fig. 1, are replaced with a switching cell (Fig. 2). The mean value of the current $I_{D1}$ is controlled by the referent signal $I_r$, so the switching cell acts like a controllable current source supplying the output RC circuit. The basic idea of the injected and absorbed current method is to calculate the mean value of the current $I_{D1}$, which creates a voltage drop in the output RC circuit, and then calculate its total differential. The procedure is applied for the continuous and separately for the discontinuous conduction mode.

### 2.1. Continuous conduction mode

The inductor current in the continuous conduction mode never falls to zero. In steady state conditions, assuming constant output voltage (infinite output capacity) and ideal components, the relation between input and output voltage is given by [23]:

$$\frac{V_{out}}{V_{in}} = \frac{1}{1-D}, \tag{1}$$

where:

- $V_{in}$ – converter input voltage (V),
- $V_{out}$ – converter output voltage (V),
- $D$ – duty cycle.

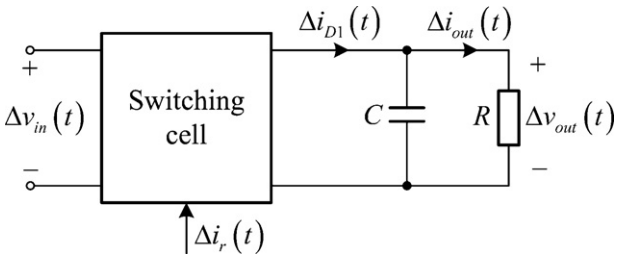


**Fig. 2.** The dynamic model of the DC/DC boost converter in peak current mode control.

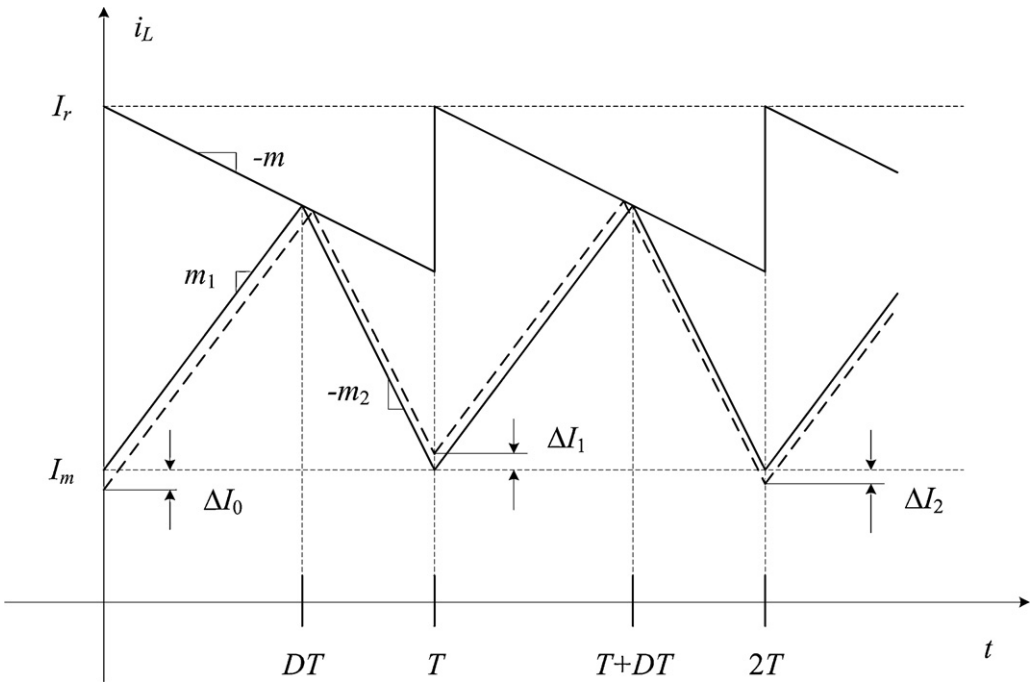


**Fig. 3.** The waveforms of the boost converter inductor current with compensation ramp in continuous conduction mode.

To compensate for the well known instability of the boost converter for duty cycle values greater than 0.5, a compensation ramp is used [23]. The waveforms of the boost converter with the compensation ramp in continuous conduction mode are shown in Fig. 3.

According to Fig. 3, successive variations of current can be determined by:

$$\Delta I_n = \left(-\frac{m_2 - m}{m_1 + m}\right)^n \cdot \Delta I_0, \tag{2}$$

where:

- $m$ – slope of the compensation ramp ($As^{-1}$),
- $m_1$ – slope of the inductor current rising part ($As^{-1}$),
- $m_2$ – slope of the inductor current falling part ($As^{-1}$),
- $\Delta I_0$ – initial variation of the inductor current (A),
- $\Delta I_n$ – $n$th successive variation of the inductor current (A),
- $n$ – ordinal number of successive variation.

The current variation $\Delta I_n$ vanishes with time, i.e. the converter is stabilized, if the expression under $n$th power is less than 1, or if:

$$m > \frac{m_2 - m_1}{2}. \tag{3}$$

The inductor current $i_L$ and diode current $i_{D1}$ waveforms in the continuous conduction mode with compensation ramp are shown in Fig. 4.

The slope of the inductor current $i_L$ rising part, according to Fig. 4, is determined by:

$$m_1 = \frac{I_r - I_m}{DT} - m = \frac{V_{in}}{L}, \tag{4}$$

where:

- $I_r$ – referent inductor current (A), or control signal (mA) or (V),
- $I_m$ – minimal inductor current at the beginning of switching period (A),
- $I_f$ – minimal inductor current at the end of switching period (A),
- $T$ – constant switching period (s),
- $L$ – inductor inductance (H).

From (4) the duty cycle $D$ follows:

$$D = \frac{L}{T} \cdot \frac{I_r - I_m}{V_{in} + mL}. \tag{5}$$

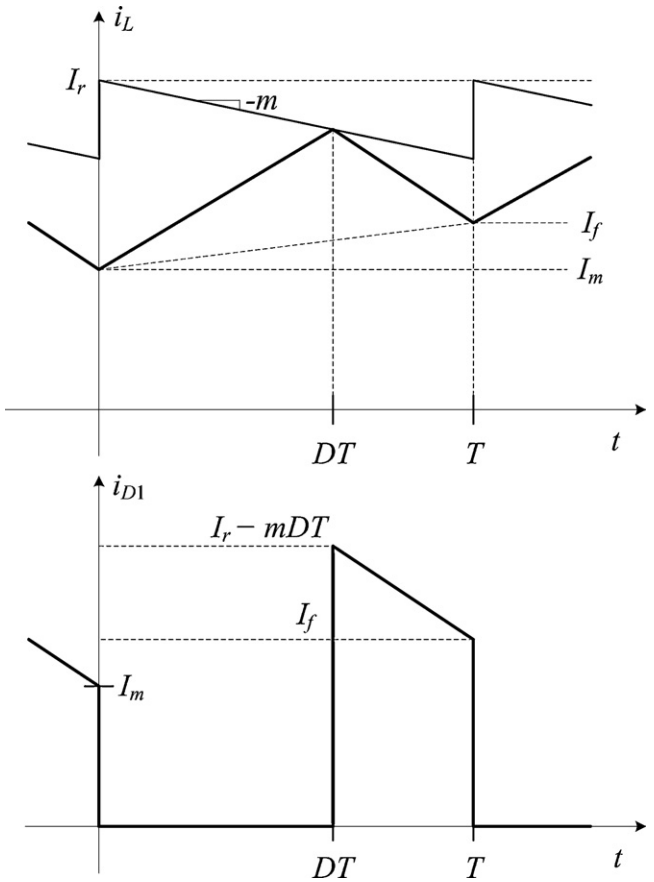


**Fig. 4.** The waveforms of the inductor current $i_L$ and diode current $i_{D1}$ in continuous conduction mode with compensation ramp.

The slope of the inductor current $i_L$ falling part, according to Fig. 4, is determined by:

$$m_2 = \frac{I_r - I_f}{(1-D)T} - \frac{mD}{1-D} = \frac{V_{out} - V_{in}}{L}. \tag{6}$$

From (6) the expression for $I_f$ follows:

$$I_f = I_r - \frac{T}{L}(V_{out} - V_{in})(1-D) - mDT. \tag{7}$$

Inserting (5) into (7) results in:

$$I_f = I_r - \frac{T}{L}(V_{out} - V_{in}) + \frac{I_r - I_m}{V_{in} + mL}(V_{out} - V_{in} - mL). \tag{8}$$

The change of minimal current value $I_m$, according to Fig. 4, is described by:

$$\frac{dI_m}{dt} = \frac{I_f - I_m}{T}. \tag{9}$$

Inserting (8) into (9), results in:

$$\frac{dI_m}{dt} = \frac{1}{T}\frac{V_{out}}{V_{in} + mL}(I_r - I_m) - \frac{1}{L}(V_{out} - V_{in}). \tag{10}$$

The total differential of change of $I_m$ is given by:

$$d\frac{dI_m}{dt} = k_{21} \cdot dI_r + k_{22} \cdot dI_m + k_{23} \cdot dV_{in} + k_{24} \cdot dV_{out}, \tag{11}$$

where:

$$\begin{aligned}
k_{21} &= \frac{\partial(dI_m)/(dt)}{\partial I_r} = \frac{1}{T}\frac{V_{out}}{V_{in} + mL},\\
k_{22} &= \frac{\partial(dI_m)/(dt)}{\partial I_m} = -\frac{1}{T}\frac{V_{out}}{V_{in} + mL},\\
k_{23} &= \frac{\partial(dI_m)/(dt)}{\partial V_{in}} = \frac{1}{L} - \frac{1}{T}\frac{V_{out}}{(V_{in} + mL)^2}(I_r - I_m),\\
k_{24} &= \frac{\partial(dI_m)/(dt)}{\partial V_{out}} = \frac{1}{T}\frac{I_r - I_m}{V_{in} + mL} - \frac{1}{L}.
\end{aligned} \tag{12}$$

Replacing the differential operator $d$ in (11), by small changes $\Delta$ arround the operating point, and applying Laplace transform on expression (11), results in:

$$\begin{aligned}
s \cdot \Delta i_m(s) = {} & k_{21} \cdot \Delta i_r(s) + k_{22} \cdot \Delta i_m(s) + k_{23} \cdot \Delta v_{in}(s)\\
& + k_{24} \cdot \Delta v_{out}(s),
\end{aligned} \tag{13}$$

from which the expression for $\Delta i_m$ follows:

$$\Delta i_m(s) = \frac{k_{21} \cdot \Delta i_r(s) + k_{23} \cdot \Delta v_{in}(s) + k_{24} \cdot \Delta v_{out}(s)}{s - k_{22}}. \tag{14}$$

The mean value of the diode current $I_{D1}$ is given by (Fig. 4):

$$I_{D1} = \frac{1}{T}\int_0^T i_{D1}(t)dt = \frac{1}{2}(1-D)(I_r - mDT + I_f). \tag{15}$$

On substituting (5) and (8) into (15), the expression for mean value of the diode current is obtained, which is also the mean value of the output RC circuit current:

$$\begin{aligned}
I_{D1} = {} & I_r - \frac{T}{2L}(V_{out} - V_{in}) - \frac{L}{T} \cdot I_r \cdot \frac{I_r - I_m}{V_{in} + mL} + \frac{V_{out} - V_{in} - mL}{V_{in} + mL}\\
& \times (I_r - I_m) - \frac{L}{2T}\frac{V_{out} - V_{in} - 2mL}{(V_{in} + mL)^2}(I_r - I_m)^2.
\end{aligned} \tag{16}$$

The total differential of the mean diode current $I_{D1}$ is determined by:

$$dI_{D1} = k_{25} \cdot dI_r + k_{26} \cdot dI_m + k_{27} \cdot dV_{in} + k_{28} \cdot dV_{out}, \tag{17}$$

where:

$$\begin{aligned}
k_{25} &= \frac{\partial I_{D1}}{\partial I_r} = 1 - \frac{L}{T}\frac{2I_r - I_m}{V_{in} + mL} + \frac{V_{out} - V_{in} - mL}{V_{in} + mL} - \frac{L}{T}\frac{V_{out} - V_{in} - 2mL}{(V_{in} + mL)^2}(I_r - I_m),\\
k_{26} &= \frac{\partial I_{D1}}{\partial I_m} = \frac{L}{T}\frac{I_r}{V_{in} + mL} - \frac{V_{out} - V_{in} - mL}{V_{in} + mL} + \frac{L}{T}\frac{V_{out} - V_{in} - 2mL}{(V_{in} + mL)^2}(I_r - I_m),\\
k_{27} &= \frac{\partial I_{D1}}{\partial V_{in}} = \frac{T}{2L} + \frac{I_r - I_m}{(V_{in} + mL)^2}\left(\frac{L}{T}I_r - V_{out}\right) + \frac{L}{2T}(I_r - I_m)^2 \cdot \frac{2V_{out} - V_{in} - 3mL}{(V_{in} + mL)^3},\\
k_{28} &= \frac{\partial I_{D1}}{\partial V_{out}} = -\frac{T}{2L} + \frac{I_r - I_m}{V_{in} + mL} - \frac{L}{2T}\frac{(I_r - I_m)^2}{(V_{in} + mL)^2}.
\end{aligned} \tag{18}$$

Replacing the differential operator $d$ in (17) with small changes $\Delta$ arround the operating point, and applying Laplace transform to (17), results in:

$$\begin{aligned}
\Delta i_{D1}(s) = {} & k_{25} \cdot \Delta i_r(s) + k_{26} \cdot \Delta i_m(s)\\
& + k_{27} \cdot \Delta v_{in}(s) + k_{28} \cdot \Delta v_{out}(s).
\end{aligned} \tag{19}$$

Substituting (14) into (19) yields:

$$\begin{aligned}
\Delta i_{D1}(s) = {} & \left(k_{25} + \frac{k_{21}k_{26}}{s - k_{22}}\right) \cdot \Delta i_r(s) + \left(k_{27} + \frac{k_{23}k_{26}}{s - k_{22}}\right)\\
& \times \cdot \Delta v_{in}(s) + \left(k_{28} + \frac{k_{24}k_{26}}{s - k_{22}}\right) \cdot \Delta v_{out}(s).
\end{aligned} \tag{20}$$

The change of output voltage $\Delta v_{out}$ is given by:

$$\Delta v_{out}(s) = \Delta i_{D1}(s) \cdot R \cdot \frac{1 + sR_CC}{1 + s(R_C + R)C}. \tag{21}$$

On substituting (20) into (21) and rearranging, the following expression is obtained:

$$\Delta v_{out}(s) = G_{i,c1}(s) \cdot \Delta i_r(s) + G_{i,c2}(s) \cdot \Delta v_{in}(s), \tag{22}$$

where:

$$\begin{aligned}
G_{i,c1}(s) &= \left.\frac{\Delta v_{out}(s)}{\Delta i_r(s)}\right|_{\Delta v_{in}=0} = \frac{k_{32}s^2 + k_{33}s + k_{34}}{k_{29}s^2 + k_{30}s + k_{31}},\\
G_{i,c2}(s) &= \left.\frac{\Delta v_{out}(s)}{\Delta v_{in}(s)}\right|_{\Delta i_r=0} = \frac{k_{35}s^2 + k_{36}s + k_{37}}{k_{29}s^2 + k_{30}s + k_{31}},
\end{aligned} \tag{23}$$

and:

$$\begin{aligned}
k_{29} &= (R_C + R)C + k_{28}RR_CC,\\
k_{30} &= 1 - k_{22}C(R_C + R) - k_{28}R + RR_CC(k_{22}k_{28} - k_{24}k_{26}),\\
k_{31} &= R(k_{22}k_{28} - k_{24}k_{26}) - k_{22},\\
k_{32} &= k_{25}RR_CC,\\
k_{33} &= RR_CC(k_{21}k_{26} - k_{22}k_{25}) + k_{25}R,\\
k_{34} &= R(k_{21}k_{26} - k_{22}k_{25}),\\
k_{35} &= k_{27}RR_CC,\\
k_{36} &= RR_CC(k_{23}k_{26} - k_{22}k_{27}) + k_{27}R,\\
k_{37} &= R(k_{23}k_{26} - k_{22}k_{27}).
\end{aligned} \tag{24}$$

By neglecting the equivalent series resistance of the capacitor $R_C$, the transfer functions (23) assume the form:

$$\begin{aligned}
G_{i,c1}(s) &= K_{i,c1} \cdot \frac{1 - T_{i,cb1}s}{1 + 2\zeta_i T_{i,c}s + T_{i,c}^2 s^2},\\
G_{i,c2}(s) &= K_{i,c2} \cdot \frac{1 + T_{i,cb2}s}{1 + 2\zeta_i T_{i,c}s + T_{i,c}^2 s^2},
\end{aligned} \tag{25}$$

where:

$$\begin{aligned}
K_{i,c1} &= \frac{k_{34}}{k_{31}}, \quad K_{i,c2} = \frac{k_{37}}{k_{31}},\\
T_{i,cb1} &= -\frac{k_{33}}{k_{34}}, \quad T_{i,cb2} = \frac{k_{36}}{k_{37}},\\
T_{i,c} &= \sqrt{\frac{k_{29}}{k_{31}}}, \quad \zeta_i = \frac{k_{30}}{2\sqrt{k_{29}k_{31}}}.
\end{aligned} \tag{26}$$

By the choice of a much higher switching frequency than the frequency of the output RC circuit, the transfer function (25) poles become real, i.e. $\zeta_i > 1$, so the transfer functions (25) can be written as:

$$G_{i,c1}(s) = K_{i,c1} \cdot \frac{1 - T_{i,cb1}s}{(1 + T_{i,c1}s)(1 + T_{i,c2}s)},$$
$$G_{i,c2}(s) = K_{i,c2} \cdot \frac{1 + T_{i,cb2}s}{(1 + T_{i,c1}s)(1 + T_{i,c2}s)}, \quad (27)$$

where:

$$T_{i,c1} = \frac{T_{i,c}}{\zeta_i - \sqrt{\zeta_i^2 - 1}},$$
$$T_{i,c2} = \frac{T_{i,c}}{\zeta_i + \sqrt{\zeta_i^2 - 1}}. \quad (28)$$

Furthermore, if $\zeta_i \gg 1$ then from (28) it follows that $T_{i,c1} \gg T_{i,c2}$, so $T_{i,c2}$ can be neglected with respect to $T_{i,c1}$. The nonminimum-phase zero in transfer function $G_{i,c1}$ (27) can be neglected only if a relatively small value of the inductor inductance $L$ is chosen. The zero in transfer function $G_{i,c2}$ (27) can only be neglected if the equivalent series resistance of the output capacitor is neglected (ceramic capacitor in parallel with electrolyte capacitor).

It follows that by the choice of the inductance of a relatively small amount, the transfer functions (27) are simplified to the $PT_1$ form:

$$G_{i,c1}(s) = \frac{K_{i,c1}}{1 + T_{i,c1}s},$$
$$G_{i,c2}(s) = \frac{K_{i,c2}}{1 + T_{i,c1}s}. \quad (29)$$

### 2.2. Discontinuous conduction mode

The inductor current falls to zero during one switching cycle in the discontinuous conduction mode. The relation between input and output voltage in steady state conditions, assuming constant input and output voltages and ideal components, is given by [23]:

$$\frac{V_{out}}{V_{in}} = \frac{D_1 + D}{D_1}, \quad (30)$$

where: $D_1$ – a fraction of the switching cycle in which the inductor current is zero.

The waveforms of inductor current $i_L$ and diode current $i_{D1}$ in the discontinuous conduction mode with the compensation ramp are shown in Fig. 5.

The slope of the inductor current $i_L$ rising part, according to Fig. 5, is determined by:

$$m_1 = \frac{I_r}{DT} - m = \frac{V_{in}}{L}, \quad (31)$$

from which the expression for $D$ follows:

$$D = \frac{L}{T} \cdot \frac{I_r}{V_{in} + mL}. \quad (32)$$

The slope of the inductor current $i_L$ falling part, according to Fig. 5, is determined by:

$$m_2 = \frac{I_r}{D_1 T} - m \cdot \frac{D}{D_1} = \frac{V_{out} - V_{in}}{L}, \quad (33)$$

where $D_1$ is marked in Fig. 5. From (33) the expression for $D_1$ follows:

$$D_1 = \frac{L}{T} \cdot \frac{I_r - mDT}{V_{out} - V_{in}}. \quad (34)$$

Substituting (32) into (34), results in:

$$D_1 = \frac{L}{T} \cdot \frac{I_r}{V_{out} - V_{in}} \cdot \frac{V_{in}}{V_{in} + mL}. \quad (35)$$

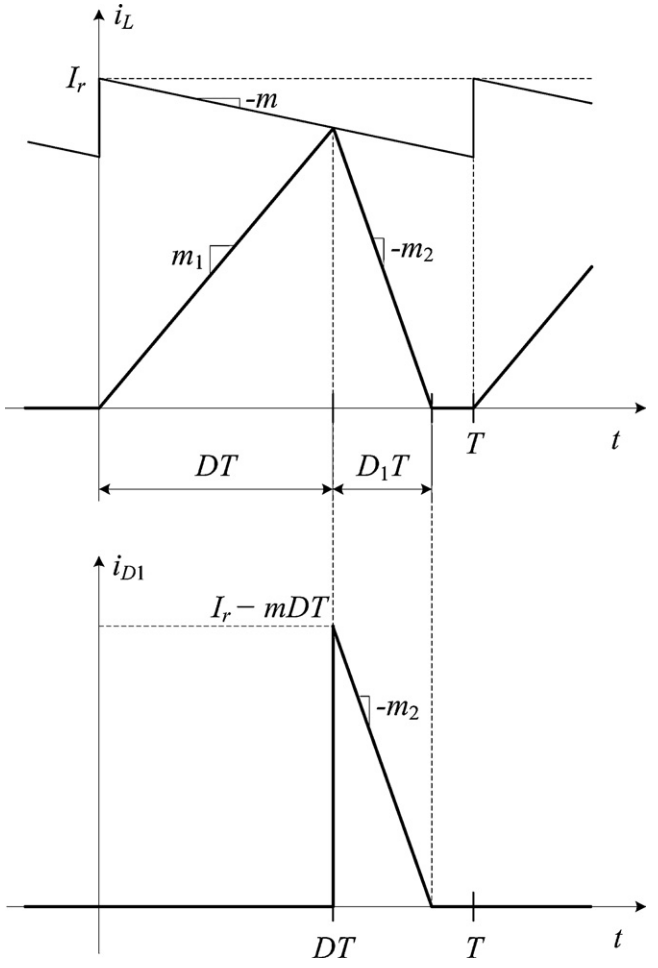


**Fig. 5.** The waveforms of inductor current $i_L$ and diode current $i_{D1}$ in discontinuous conduction mode with compensation ramp.

The diode current mean value $I_{D1}$ is determined by (Fig. 5):

$$I_{D1} = \frac{1}{2} D_1 (I_r - mDT). \quad (36)$$

Substituting (32) and (35) into (36), results in:

$$I_{D1} = \frac{L}{2T} \cdot \frac{I_r^2}{V_{out} - V_{in}} \cdot \frac{V_{in}^2}{(V_{in} + mL)^2}. \quad (37)$$

The total differential of the diode current mean value $I_{D1}$ has the form:

$$dI_{D1} = k_{38} dI_r + k_{39} dV_{in} + k_{40} dV_{out}, \quad (38)$$

where:

$$k_{38} = \frac{\partial I_{D1}}{\partial I_r} = \frac{L}{T} \cdot \frac{V_{in}^2 \cdot I_r}{(V_{out} - V_{in})(V_{in} + mL)^2},$$
$$k_{39} = \frac{\partial I_{D1}}{\partial V_{in}} = \frac{L V_{in} I_r^2}{2T} \cdot \frac{V_{in}^2 + mL(2V_{out} - V_{in})}{(V_{out} - V_{in})^2 (V_{in} + mL)^3}, \quad (39)$$
$$k_{40} = \frac{\partial I_{D1}}{\partial V_{out}} = -\frac{L}{2T} \cdot \frac{V_{in}^2 \cdot I_r^2}{(V_{in} + mL)^2 (V_{out} - V_{in})^2}.$$

Replacing the differential operator $d$ in (38) with small changes $\Delta$ arround the operating point, and applying Laplace transform to (38), results in expression for the small changes of output RC circuit current mean value:

$$\Delta i_{D1}(s) = k_{38} \Delta i_r(s) + k_{39} \Delta v_{in}(s) + k_{40} \Delta v_{out}(s). \quad (40)$$

The change of output voltage $\Delta v_{out}$ is obtained by multiplying $\Delta i_{D1}$ and output circuit impedance:

$$\Delta v_{out}(s) = \Delta i_{D1}(s) \cdot R \cdot \frac{1 + sR_C C}{1 + s(R_C + R)C}. \tag{41}$$

On expressing the $\Delta i_{D1}$ from (41) and inserting it into (40), the change of output voltage is obtained:

$$\Delta v_{out}(s) = G_{i,d1}(s) \cdot \Delta i_r(s) + G_{i,d2}(s) \cdot \Delta v_{in}(s), \tag{42}$$

where:

$$\begin{aligned} G_{i,d1}(s) &= \left.\frac{\Delta v_{out}(s)}{\Delta i_r(s)}\right|_{\Delta v_{in}=0} = \frac{K_{i,d1}}{1 + T_{i,d}s}, \\ G_{i,d2}(s) &= \left.\frac{\Delta v_{out}(s)}{\Delta v_{in}(s)}\right|_{\Delta i_r=0} = \frac{K_{i,d2}}{1 + T_{i,d}s}, \end{aligned} \tag{43}$$

are the appropriate transfer functions in the discontinuous conduction mode, with parameters:

$$\begin{aligned} K_{i,d1} &= \frac{k_{38}R(1 + R_C C)}{1 - k_{40}R}, \\ K_{i,d2} &= \frac{k_{39}R(1 + R_C C)}{1 - k_{40}R}, \\ T_{i,d} &= \frac{R_C + R}{1 - k_{40}R}C. \end{aligned} \tag{44}$$

It is important to notice that with careful converter design the transfer functions for continuous (29) and discontinuous (43) conduction modes have the same $PT_1$ form, with different parameters.

## 3. Modeling of PEM fuel cells

The fuel cell is an electrochemical device that directly converts the chemical energy of the fuel (usually hydrogen) into electricity. The byproducts of the reaction are water and heat. The basic electrochemical reactions are described by:

- Anode:

$$H_2 \rightarrow 2H^+ + 2e^-, \tag{45}$$

- Cathode:

$$\frac{1}{2}O_2 + 2H^+ + 2e^- \rightarrow H_2O, \tag{46}$$

- Overall reaction:

$$H_2 + \frac{1}{2}O_2 \rightarrow H_2O. \tag{47}$$

The single cell voltage can be described by [31]:

$$V_{cell} = E - V_{act} - V_{ohm} - V_{con}. \tag{48}$$

The thermodynamic or the Nernst potential $E$ of the cell represents its reversible voltage, and is given by [32]:

$$E = 1.482 - 8.45 \cdot 10^{-4} \cdot T + 4.31 \cdot 10^{-5} \cdot T \cdot \ln(p_{H_2} \cdot p_{O_2}^{0.5}). \tag{49}$$

The voltage drop due to the activation of the anode and cathode, also known as the activation overpotential, is given by:

$$V_{act} = -[\xi_1 + \xi_2 \cdot T + \xi_3 \cdot T \cdot \ln(C_{O_2}) + \xi_4 \cdot T \cdot \ln(I_{FC})], \tag{50}$$

where:

- $I_{FC}$ – fuel cell current (A),
- $\xi_{1-4}$ – cell parameters, whose values are defined based on theoretical equations with kinetic, thermodynamic and electrochemical foundations [33],
- $C_{O_2}$ – oxygen concentration in the catalytic interface of the cathode (mol cm$^{-3}$), defined by:

$$C_{O_2} = \frac{p_{O_2}}{5.08 \cdot 10^6 \cdot \exp(-498/T)}. \tag{51}$$

The parameter $\xi_2$ is determined by [31]:

$$\xi_2 = 0.00286 + 0.0002 \ln(A) + 4.3 \cdot 10^{-5} \cdot \ln(C_{H_2}), \tag{52}$$

where $C_{H_2}$ is determined by:

$$C_{H_2} = \frac{p_{H_2}}{5.08 \cdot 10^6 \cdot \exp(-498/T)}. \tag{53}$$

The resistive or the ohmic losses result from the resistance to proton transfer through the membrane and the resistance to the electron transfer through the electrodes:

$$V_{ohm} = I_{FC} \cdot (R_M + R_C) = I_{FC} \cdot R_{ohm}, \tag{54}$$

where $R_C$ is the resistance to the electron trransfer through the electrodes, usually constant, and $R_M$ is the membrane equivalent resistance, defined by [31]:

$$R_M = \frac{\rho_M \cdot l}{A}, \tag{55}$$

where:

- $\rho_M$ – specific resistance of the membrane ($\Omega$ cm),
- $A$ – cell active area (cm$^2$),
- $l$ – membrane thickness (cm).

Membranes of the Nafion type, considered here, are registered trademark of the Dupont company, and are widely used in the PEM fuel cells. Their specific resistance is given by [33]:

$$\rho_M = \frac{181.6 \cdot [1 + 0.03 \cdot I_{FC}/A + 0.062 \cdot (T/303)^2 (I_{FC}/A)^{2.5}]}{[\lambda_m - 0.634 - 3 \cdot I_{FC}/A] \cdot \exp[4.18 \cdot (T - 303/T)]} \tag{56}$$

where $\lambda_m$ is the parameter which determines the average water content in the membrane, with reported values arround 14–23 in conditions of 100% membrane humidity.

The concentration polarization or the voltage drop due to mass transport occurs when the reactant is rapidly consumed in the electrochemical reaction, so it is necessary to quickly deliver more reactant to the reaction site. Given the limited permeability of the electrodes, there is a concentration gradient of the reactant. This occurs at higher currents, because it is known that the amount of hydrogen consumed (in mols per second) is directly proportional to the fuel cell current:

$$\dot{n}_{H_2} = \frac{I_{FC}}{2F}. \tag{57}$$

Therefore, the maximum current density $J_{max}$ (A cm$^{-2}$) is defined, which corresponds to the maximum delivery rate of the reactant in the reaction (catalytic) layer. The fuel cell is designed so as to have as great a value of maximum current density $J_{max}$ as possible. Typical values range from 0.5 to 2 A cm$^{-2}$, while carefully designed fuel cells can provide up to 3 A cm$^{-2}$.

Thus, the voltage drop due to concentration polarization can be associated with the current density in the following way [31]:

$$V_{con} = -B \cdot \ln\left(1 - \frac{J}{J_{max}}\right) = -B \cdot \ln\left(1 - \frac{I_{FC}}{J_{max} \cdot A}\right), \tag{58}$$

where:

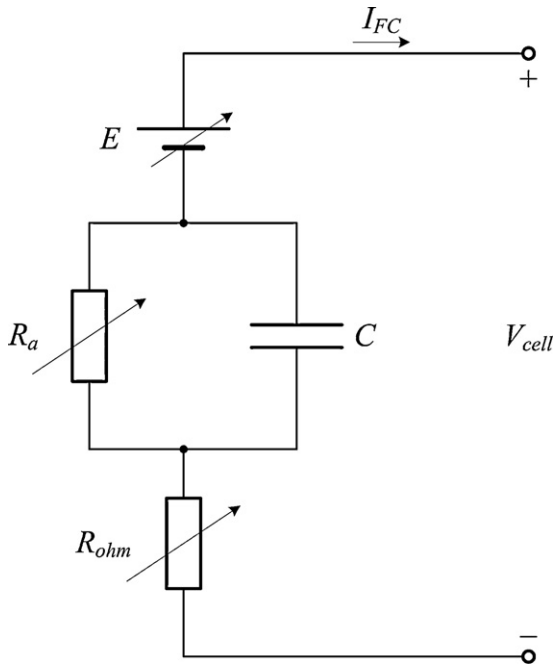


**Fig. 6.** The equivalent electrical scheme of the dynamic fuel cell model.

- $B$ – fuel cell parameter (V),
- $J$ – fuel cell current density ($A\,cm^{-2}$).

The fuel cell dynamics can be described by first order delay in the activation and concentration polarization [31], with associated time constant:

$$\tau = C \cdot R_a, \tag{59}$$

where $C$ represents the cell equivalent capacitance in Farads, while $R_a$ represents the equivalent resistance in Ω. The capacitance value $C$ usually has a constant value of several Farads, while the resistance value can be determined as:

$$R_a = \frac{V_{act} + V_{con}}{I_{FC}}. \tag{60}$$

Fig. 6 shows the equivalent electrical scheme of the dynamic fuel cell model. From Fig. 6 it follows:

$$V_{cell} = E - V_C - V_{ohm}, \tag{61}$$

where $V_C$ is the capacitor's $C$ voltage (Fig. 6), determined by the differential equation:

$$\frac{dV_C}{dt} = \frac{I_{FC}}{C}\left(1 - \frac{V_C}{V_{act} + V_{con}}\right). \tag{62}$$

The voltage of the whole stack is determined by:

$$V_{FC} = N_c \cdot V_{cell}, \tag{63}$$

where $N_c$ is the total number of cells in the fuel cell stack.

### 3.1. Linearized fuel cell model

The linearized fuel cell model, suitable for controller design purposes, is derived and/or described in [1,34,35]. Due to the completeness and some minor differences, the linear model will be derived once again in the following lines.

From the previously derived equations, it is evident that the voltage of the fuel cell is a function of several variables:

$$V_{FC} = f(I_{FC}, T, p_{H_2}, p_{O_2}). \tag{64}$$

Since changes in pressure of the reactants in the models of voltage losses are taken into account through semiempirical relations, the pressures of the reactants actually become the constants of nonlinear and linear models. Furthermore, the voltage dependence on temperature is significant, but with a dynamic point of view it is irrelevant, because the temperature of the fuel cell must be regulated [36,37], and hence it can be considered constant. It is therefore necessary to find a linear model of voltage dependence on fuel cell current:

$$V_{FC} = f(I_{FC}). \tag{65}$$

The Nernst voltage does not depend on the fuel cell current, so it can be written as:

$$E = g_1 = 1.482 - 8.45 \cdot 10^{-4} \cdot T + 4.31 \cdot 10^{-5} \cdot T \cdot \ln(p_{H_2} \cdot p_{O_2}^{0.5}). \tag{66}$$

The activation voltage drop (50) depends on the fuel cell current, so the expression (50) can be written as:

$$V_{act} = g_2 + g_3 \ln(I_{FC}), \tag{67}$$

where:

$$\begin{aligned} g_2 &= -(\xi_1 + \xi_2 T + \xi_3 T \ln(C_{O_2})), \\ g_3 &= -\xi_4 T, \end{aligned} \tag{68}$$

where parameter $\xi_2$ is determined by expressions (52) and (53), and concentration $C_{O_2}$ is determined by (51).

The concentration polarization also depends on the fuel cell current (58), so it can be written as:

$$V_{con} = g_4 \ln(1 + g_5 I_{FC}), \tag{69}$$

where:

$$\begin{aligned} g_4 &= -B, \\ g_5 &= -\frac{1}{J_{max} \cdot A}. \end{aligned} \tag{70}$$

From (54), (55) and (56), ohmic voltage drop can be written as:

$$V_{ohm} = I_{FC}\left(g_6 + \frac{g_7 + g_8 I_{FC} + g_9 I_{FC}^{2.5}}{g_{10} + g_{11} I_{FC}}\right), \tag{71}$$

where:

$$\begin{aligned} g_6 &= R_C, \\ g_7 &= 181.6 \cdot \frac{l}{A}, \\ g_8 &= 5.448 \cdot \frac{l}{A^2}, \\ g_9 &= 1.2264 \cdot 10^{-4} \cdot \frac{lT^2}{A^{3.5}}, \\ g_{10} &= (\lambda_m - 0.634) \cdot \exp\left[4.18 \cdot \left(\frac{T - 303}{T}\right)\right], \\ g_{11} &= -\frac{3}{A} \cdot \exp\left[4.18 \cdot \left(\frac{T - 303}{T}\right)\right]. \end{aligned} \tag{72}$$

Substituting (67) and (69) into (62), results in:

$$\frac{dV_C}{dt} = \frac{I_{FC}}{C}\left(1 - \frac{V_C}{g_2 + g_3 \ln(I_{FC}) + g_4 \ln(1 + g_5 I_{FC})}\right). \tag{73}$$

The change of voltage $V_C$ (73) is a function of two variables, $I_{FC}$ and $V_C$ itself, so its total differential is:

$$d\frac{dV_C}{dt} = g_{12} \cdot dI_{FC} + g_{13} \cdot dV_C, \tag{74}$$

where:

$$\begin{aligned} g_{12} &= \frac{\partial(dV_C)/(dt)}{\partial I_{FC}} = \frac{I_{FC}}{C} \cdot \frac{(g_3)/(I_{FC}) + (g_4 g_5)/(1 + g_5 I_{FC})}{g_2 + g_3 \ln(I_{FC}) + g_4 \ln(1 + g_5 I_{FC})}, \\ g_{13} &= \frac{\partial(dV_C)/(dt)}{\partial V_C} = -\frac{1}{C} \cdot \frac{I_{FC}}{g_2 + g_3 \ln(I_{FC}) + g_4 \ln(1 + g_5 I_{FC})}. \end{aligned} \tag{75}$$

Substituting (66) and (71) into (61), and then in (63), results in:

$$V_{FC} = N_c \left( g_1 - V_C - I_{FC} \left( g_6 + \frac{g_7 + g_8 I_{FC} + g_9 I_{FC}^{2.5}}{g_{10} + g_{11} I_{FC}} \right) \right). \tag{76}$$

The fuel cell voltage $V_{FC}$ (76) is a function of two variables, $I_{FC}$ and $V_C$, so its total differential is:

$$dV_{FC} = g_{14} \cdot dI_{FC} + g_{15} \cdot dV_C, \tag{77}$$

where:

$$\begin{aligned} g_{14} &= \frac{\partial V_{FC}}{\partial I_{FC}} = -N_c \left( g_6 + \frac{g_7 + g_8 I_{FC} + g_9 I_{FC}^{2.5}}{g_{10} + g_{11} I_{FC}} \right) \\ &\quad - N_c I_{FC} \cdot \frac{(g_8 I_{FC} + 2.5 g_9 I_{FC}^{1.5})(g_{10} + g_{11} I_{FC})}{(g_{10} + g_{11} I_{FC})^2} \\ &\quad + N_c I_{FC} g_{11} \cdot \frac{g_7 + g_8 I_{FC} + g_9 I_{FC}^{2.5}}{(g_{10} + g_{11} I_{FC})^2}, \\ g_{15} &= \frac{\partial V_{FC}}{\partial V_C} = -N_c. \end{aligned} \tag{78}$$

Replacing the differential operator $d$ with small changes $\Delta$ arround the operating point, and applying Laplace transform to (74) and (77) and rearranging, results in the transfer function of the fuel cell:

$$G_{FC}(s) = \frac{\Delta v_{FC}(s)}{\Delta i_{FC}(s)} = K_{FC} \cdot \frac{1 + T_{FC,b} s}{1 + T_{FC,1} s}, \tag{79}$$

where:

$$\begin{aligned} K_{FC} &= \frac{g_{13} g_{14} - g_{12} g_{15}}{g_{13} g_{14}}, \\ T_{FC,b} &= -\frac{g_{13} g_{14} - g_{12} g_{15}}{g_{13} g_{14}}, \\ T_{FC,1} &= -\frac{1}{g_{13}}. \end{aligned} \tag{80}$$

## 4. Integrated process model

Integration of nonlinear fuel cell model and the boost converter is done simply by connecting the inductor current signal $I_L$ to the current input of the fuel cell $I_{FC}$, and connecting the fuel cell voltage signal $V_{FC}$ to the input of the boost converter $V_{in}$.

Unlike the integration of nonlinear models, the integration of the linearized models necessary for designing the control circuit cannot be implemented directly. The reason is that the linearized model of the boost converter does not contain the inductor current $i_L$, but the referent current $I_r$. It is therefore necessary to find a connection between the inductor mean current $I_L$ and the referent current $I_r$, and include it in the linearized model with parameter $\rho$ (Fig. 7).

The mean value of boost converter inductor current in the continuous conduction mode, according to Fig. 4, is:

$$\begin{aligned} I_{L,c} &= \frac{1}{2} \cdot \frac{L}{T} \cdot \frac{I_r - I_m}{V_{in} + mL} \cdot I_m + \frac{1}{2} I_r - \frac{1}{2} mL \cdot \frac{I_r - I_m}{V_{in} + mL} \\ &\quad + \frac{1}{2} \left( 1 - \frac{L}{T} \cdot \frac{I_r - I_m}{V_{in} + mL} \right) \cdot \left( I_r - \frac{T}{L} (V_{out} - V_{in}) \right) \\ &\quad + \frac{1}{2} \left( 1 - \frac{L}{T} \cdot \frac{I_r - I_m}{V_{in} + mL} \right) \cdot \left( \frac{I_r - I_m}{V_{in} + mL} \cdot (V_{out} - V_{in} - mL) \right). \end{aligned} \tag{81}$$

Parameter $\rho$ for continuous conduction mode ($\rho = \rho_c$) is:

$$\begin{aligned} \rho_c &= \frac{\partial I_{L,c}}{\partial I_r} = \frac{1}{2} \left( 1 + \frac{L}{T} \cdot \frac{I_m - mL}{V_{in} + mL} \right) \\ &\quad + \frac{1}{2} \left[ -\frac{1}{T} \cdot \frac{L}{V_{in} + mL} \cdot \left( I_r - \frac{T}{L} (V_{out} - V_{in}) \right) \right] \\ &\quad + \frac{1}{2} \left[ -\frac{1}{T} \frac{L}{V_{in} + mL} \left( \frac{I_r - I_m}{V_{in} + mL} (V_{out} - V_{in} - mL) \right) \right] \\ &\quad + \frac{1}{2} \cdot \frac{V_{out}}{V_{in} + mL} \cdot \left( 1 - \frac{L}{T} \cdot \frac{I_r - I_m}{V_{in} + mL} \right). \end{aligned} \tag{82}$$

The mean value of boost converter inductor current in the discontinuous conduction mode, according to Fig. 5, is:

$$I_{L,d} = \frac{1}{2} \cdot \frac{L}{T} \cdot \frac{V_{out} V_{in}}{V_{out} - V_{in}} \cdot \frac{I_r^2}{(V_{in} + mL)^2}. \tag{83}$$

Parameter $\rho$ for discontinuous conduction mode ($\rho = \rho_d$) is:

$$\rho_d = \frac{\partial I_{L,d}}{\partial I_r} = \frac{L}{T} \cdot \frac{V_{out} V_{in}}{V_{out} - V_{in}} \cdot \frac{I_r}{(V_{in} + mL)^2}. \tag{84}$$

The transfer function of the whole system, according to Fig. 7, is:

$$G(s) = \frac{\Delta v_{out}(s)}{\Delta i_r(s)} = G_{i,1}(s) + \rho \cdot G_{FC}(s) \cdot G_{i,2}(s). \tag{85}$$

The transfer function of the fuel cell has the form (79), while the boost converter transfer functions have the $PT_1$ form (29) or (43), depending on the conduction mode:

$$\begin{aligned} G_{i,1}(s) &= \frac{K_{i,1}}{1 + T_i s}, \\ G_{i,2}(s) &= \frac{K_{i,2}}{1 + T_i s}. \end{aligned} \tag{86}$$

Substituting (79) and (86) into (85), results in the transfer function of the integrated system in the operating point:

$$G(s) = \frac{\Delta v_{out}(s)}{\Delta i_r(s)} = K \cdot \frac{1 + T_b s}{(1 + T_1 s)(1 + T_2 s)}, \tag{87}$$

where parameters in the operating point are:

$$\begin{aligned} K &= K_{i,1} + \rho K_{FC} K_{i,2}, \\ T_b &= \frac{K_{i,1} T_{FC,1} + \rho K_{FC} K_{i,2} T_{FC,b}}{K_{i,1} + \rho K_{FC} K_{i,2}}, \\ T_1 &= T_{FC,1}, \\ T_2 &= T_i. \end{aligned} \tag{88}$$

After obtaining the dynamic model of the whole system, it would be convenient to run some simulations that would confirm the obtained theoretical results. However, the simulations of the nonlinear model of the converter in MATLAB – SIMULINK require very small step size in a numerical integration method. According to the authors' experience, a variable step solver should be used, with the maximum step size of $1/f/200$ for the discontinuous and even smaller for the continuous conduction mode ($1/f/500$), where $f$ is the switching frequency of the converter. This leads to very slow simulations and rapid consumption of the computer memory. It is often impossible to get the converter to the operating point (starting from zero initial conditions) and then apply the request for a step change around the operating point to record the transient. It helps to use a specialized software (Spice engine based), but they lack of support for other components, like the fuel cell in our example. Calculation of necessary initial conditions to be in the operating point immediately is possible, but only for mean values of the inductor current and input and output voltages, so it is still inevitable to adjust the initial conditions manually, which is very time consuming due to the very slow simulations. Therefore, the authors decided to build the special version of the converter which enables all the experiments that would usually be done through computer simulations. The experimental system and identification of its parameters are described in the next section of the paper.

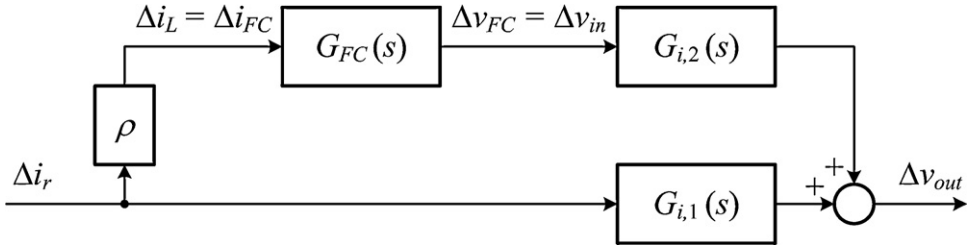


**Fig. 7.** Block diagram of the entire linearized system.

**Fig. 8.** The part of the hydrogen facility in the Laboratory for Renewable Energy Sources – LARES.

## 5. Experimental identification of the control system parameters

The control system, installed in the Laboratory for Renewable Energy Sources (LARES) [38], consists of a 500 W fuel cell BCS 64-32 (Fig. 8), manufactured by BCS Fuel Cells Inc., a 450 W boost converter specifically designed and built in the Croatian company Mareton Power Electronics (Fig. 9), a Magna Power Electronics fuel cell emulator (Fig. 10) [39,40], and finally a Compact RIO (cRIO) 9024 digital controller with input–output modules, manufactured by the National Instruments company, which will be used for the experimental identification of the system parameters and implementation of digital control algorithms [41,42].

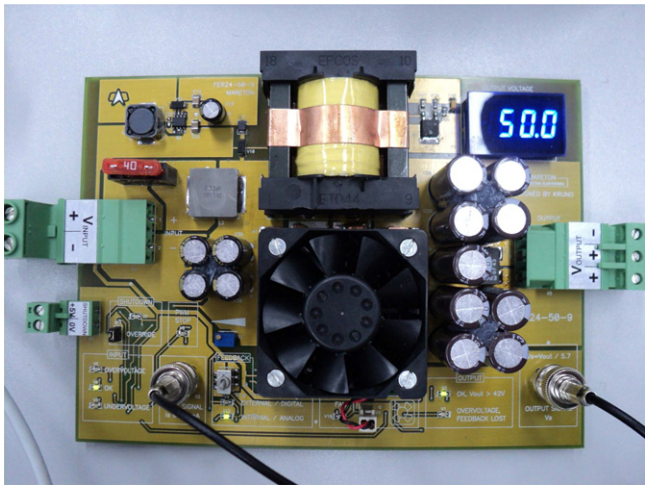

**Fig. 9.** DC/DC boost converter, designed in Mareton Power Electronics.

### 5.1. Experimental identification of the boost converter parameters

A conceptual scheme of the boost converter, built in Mareton Power Electronics, is shown in Fig. 11.

The converter is designed for the input voltage range 19–31 V and nominal output voltage 50 V. The switching frequency is constant and set to 100 kHz. The declared efficiency is 97% minimum. The nominal output current equals 9 A, while the maximum allowed current equals 13 A.

Experimental identification of the boost converter is carried out in several operating points, determined by the output current $I_{out}$. The output current of the converter in the normal operating conditions ranges in the interval $I_{out} \in [I_{out,min}, I_{out,max}]$.

The first operating point is determined by the converter output current $I_{out} = I_{out,min}$, and the last by $I_{out} = I_{out,max}$. The first operating point represents the minimum energy consumption of the system. It is assumed that a viable system design can provide the amount of power required to supply additional components (compressor or blower, the cooling unit and a system for humidifying gases if present) to be about 10 percent of the nominal power. For the fuel cell model BCS 64-32 this is a value of 2.5 A, where the boost converter output current is approximately $I_{out,min} = 1$ A. The last operating point is determined by the boost converter rated current, or nominal load of the fuel cell $I_{out,max} = 9$ A.

The output voltage is reduced to 0–10 V range by using the resistor divider with coefficient $K_{fb} = 0.176$, and the voltage feedback signal is additionally digitally filtered with time constant $T_{fb} = 350$ μs, to reduce the voltage ripple about 10 times (20 dB). Therefore, the feedback transfer function has the form:

$$G_{fb}(s) = \frac{\Delta v_{fb}(s)}{\Delta v_{out}(s)} = \frac{K_{fb}}{1 + T_{fb}s} = \frac{0.176}{1 + 0.00035s}. \quad (89)$$

**Fig. 10.** Front panels of the fuel cell emulator Magna Power Electronics and the programmable electronic load HP 6050A.

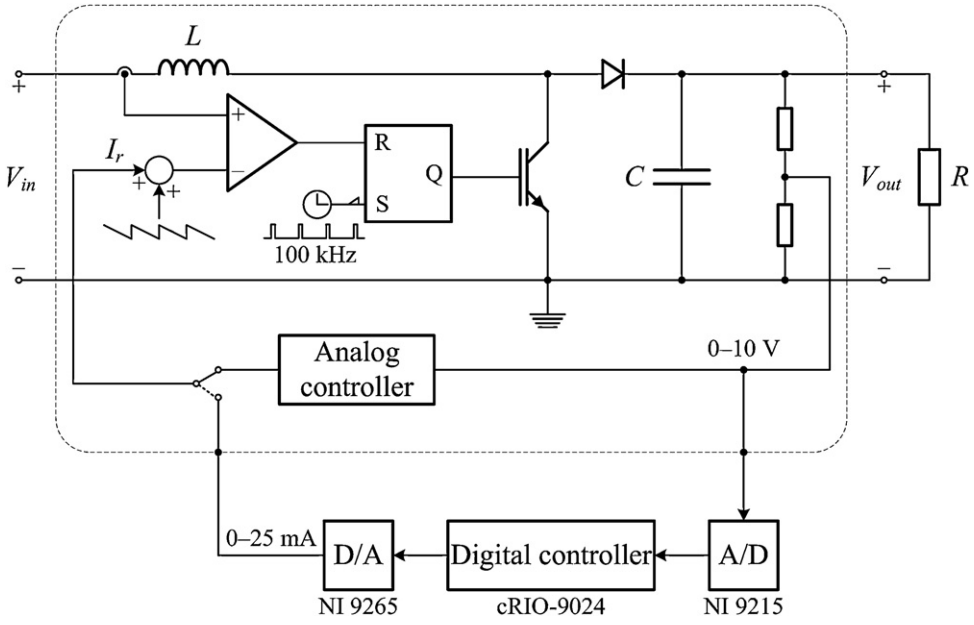


**Fig. 11.** A conceptual scheme of the boost converter, built in Mareton Power Electronics.

The transient responses for the two described (boundary) operating points are shown in Figs. 12 and 13. The responses are recorded in LabVIEW and transfered into MATLAB for easier presentation and processing of results.

Changes around the operating points are described by the linearized model (86), while the parameters of transfer functions were determined using the simplex method of optimization in MATLAB, with minimization of the ISE criterion error:

$$I_{crit} = \int_{t_1}^{t_2} (\Delta v_{out} - \Delta v_{out,lin})^2 dt, \tag{90}$$

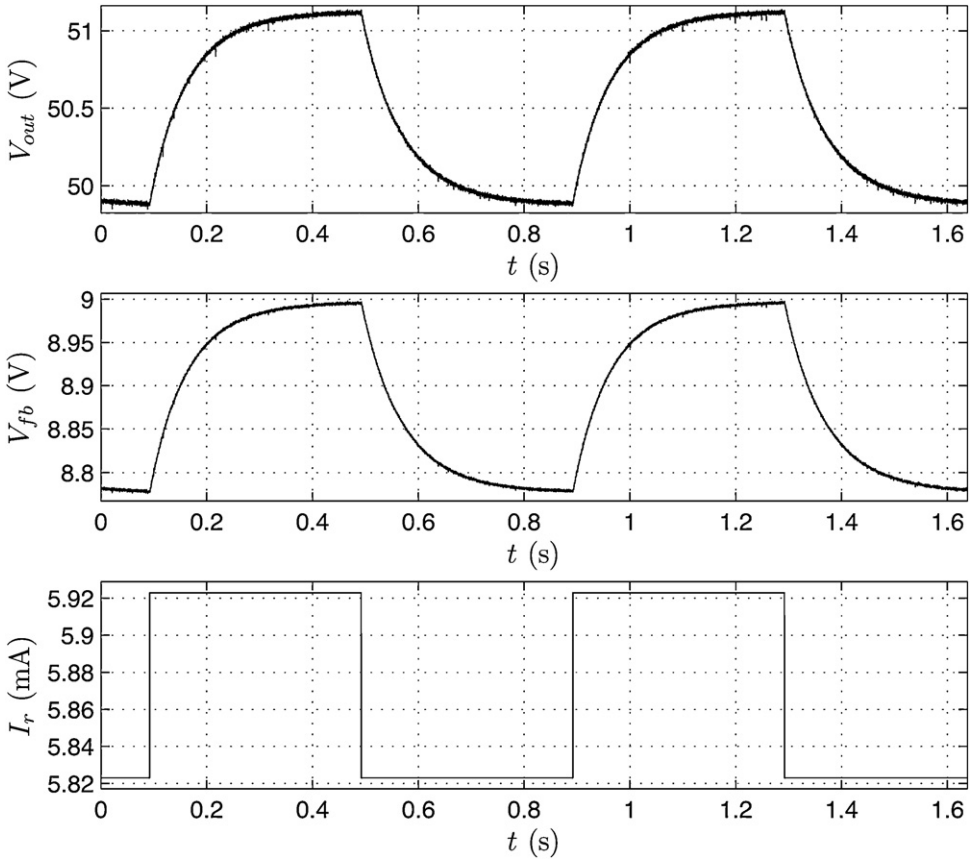


**Fig. 12.** Transient responses of the output voltage $V_{out}$ and feedback voltage $V_{fb}$ on the change of control signal $I_r(t)$, with $I_{out}$ = 1 A, $V_{in}$ = 28 V.

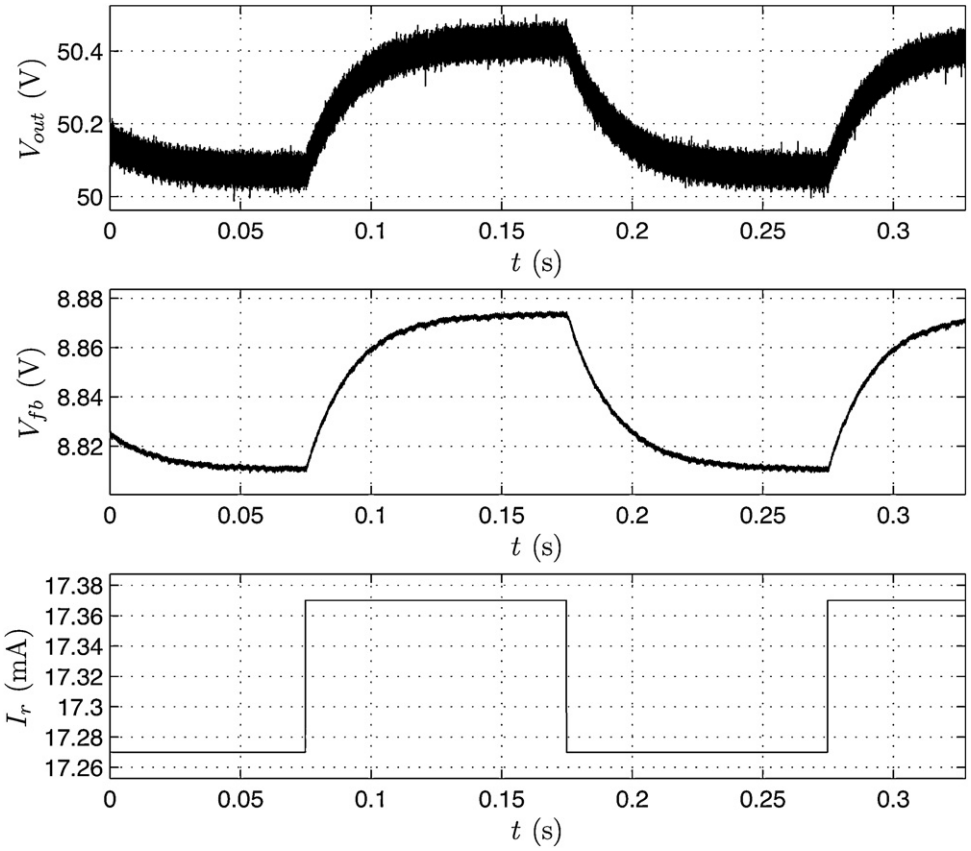


**Fig. 13.** Transient responses of the output voltage $V_{out}$ and feedback voltage $V_{fb}$ on the change of control signal $I_r(t)$, with $I_{out}$ = 9 A, $V_{in}$ = 20.5 V.

where $t_1$ and $t_2$ are initial and final simulation times, i.e. the extracted part of the recorded transients.

The recorded responses and converter linearized model transients, along with their deviations, are given in Figs. 14 and 15.

After completing the optimization procedure, the transfer function $G_{p1}$ for the first (boundary) operating point determined by $I_{out}$ = 1 A is obtained, as well as the transfer function $G_{p9}$ for the last (boundary) operating point determined by $I_{out}$ = 9 A:

$$G_{p1}(s) = \frac{\Delta v_{out}(s)}{\Delta i_r(s)} = \frac{12489}{1 + 0.0745s},$$
$$G_{p9}(s) = \frac{\Delta v_{out}(s)}{\Delta i_r(s)} = \frac{5037.5}{1 + 0.0171s}. \quad (91)$$

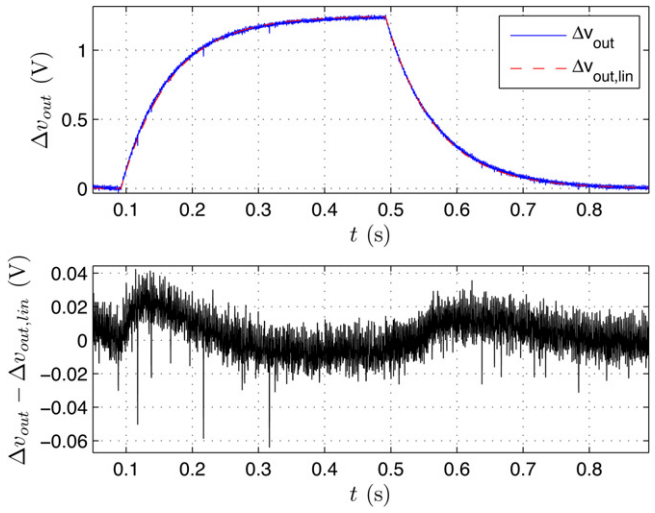


**Fig. 14.** The recorded converter output voltage transient without initial value and linearized model $G_{p1}$ (91) transient on the change of control signal $I_r(t) = 5.823 + 0.1\mathrm{S}(t - 0.092) - 0.1\mathrm{S}(t - 0.492)$ mA, with conditions described in Fig. 12 caption.

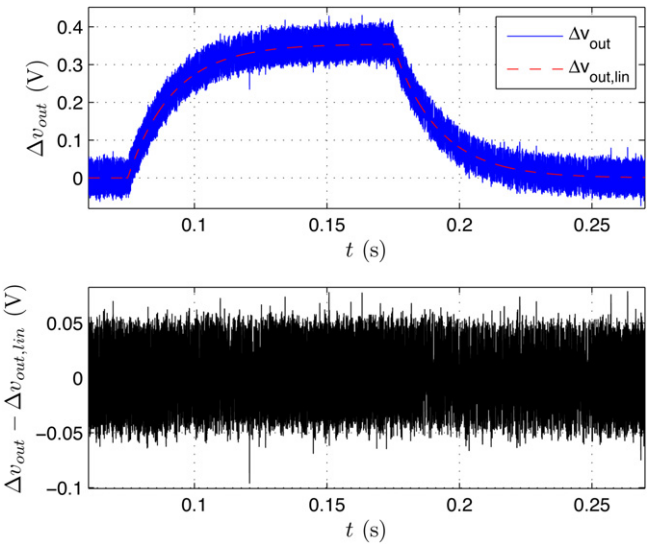


**Fig. 15.** The recorded converter output voltage transient without initial value and linearized model $G_{p9}$ (91) transient on the change of control signal $I_r(t) = 17.27 + 0.1\mathrm{S}(t - 0.075) - 0.1\mathrm{S}(t - 0.175)$ mA, with conditions described in Fig. 13 caption.

**Table 1**
The parameters of the linear model of the boost converter (86) $K_{i,1}$ and $T_i$ obtained in several operating points determined by the output current $I_{out}$.

| $I_{out}$ (A) | $V_{in}$ (V) | $K_{i,1}$ | $T_i$ (ms) |
|---|---|---|---|
| 1 | 28.0 | 12,489 | 74.5 |
| 3 | 24.7 | 7116.5 | 22.7 |
| 5 | 23.5 | 6496.8 | 19.5 |
| 7 | 22.2 | 6022.8 | 18.3 |
| 9 | 20.5 | 5037.5 | 17.1 |

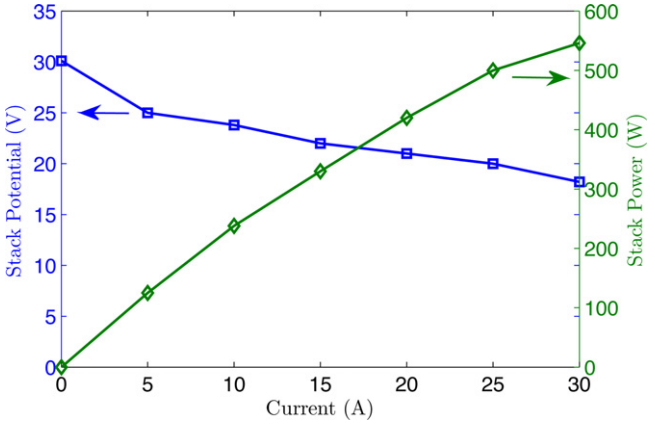


**Fig. 16.** Static *V–I* and *P–I* curve of the fuel cell BCS 64-32, obtained from the manufacturer, BCS Fuel Cells, Inc. [22].

Figs. 14 and 15 show that the maximum error of the linear model is actually determined by a standard deviation of the output voltage ripple and noise, and that the derived transfer functions (86) accurately describe the behavior of the peak current mode DC/DC boost converter.

The obtained results for all operating points are summarized in Table 1.

The transient responses in other operating points, given in Table 1, are similar to the responses in the described boundary operating points, which means that maximum error of the linear model is also determined by the standard deviation of the output voltage ripple and noise. In explanation, the transfer functions (86), along with the appropriate parameters from Table 1, accurately describe the behavior of the peak current mode DC/DC boost converter in the given operating point determined by the output current.

### 5.2. Experimental identification of the boost converter supplied with the fuel cell emulator

The boost converter supplied by the fuel cell emulator, with stored static *V–I* curve according to manufacturer's data (Fig. 16), is identified in the same operating points as the boost converter. Thereby, the fact that the boost converter is already identified is used, and its time constants are given in transfer functions (91) and in Table 1.

The responses of the boost converter supplied by the fuel cell emulator for the two described boundary operating points are shown in Figs. 17 and 18.

Changes around the operating point are described by the linearized model (87), and transfer function parameters are determined using simplex optimization method in MATLAB, by minimizing integral square error (ISE) criterion:

$$I_{crit} = \int_{t_1}^{t_2} (\Delta v_{fb} - \Delta v_{fb,lin})^2 dt, \tag{92}$$

where $t_1$ and $t_2$ are initial and final simulation times, i.e. the extracted part of the recorded transients.

The recorded transients and responses of the linearized model, together with their deviations, are shown in Figs. 19 and 20.

After optimization is carried out, the transfer functions are obtained, $G_1$ for the first (boundary) operating point determined by

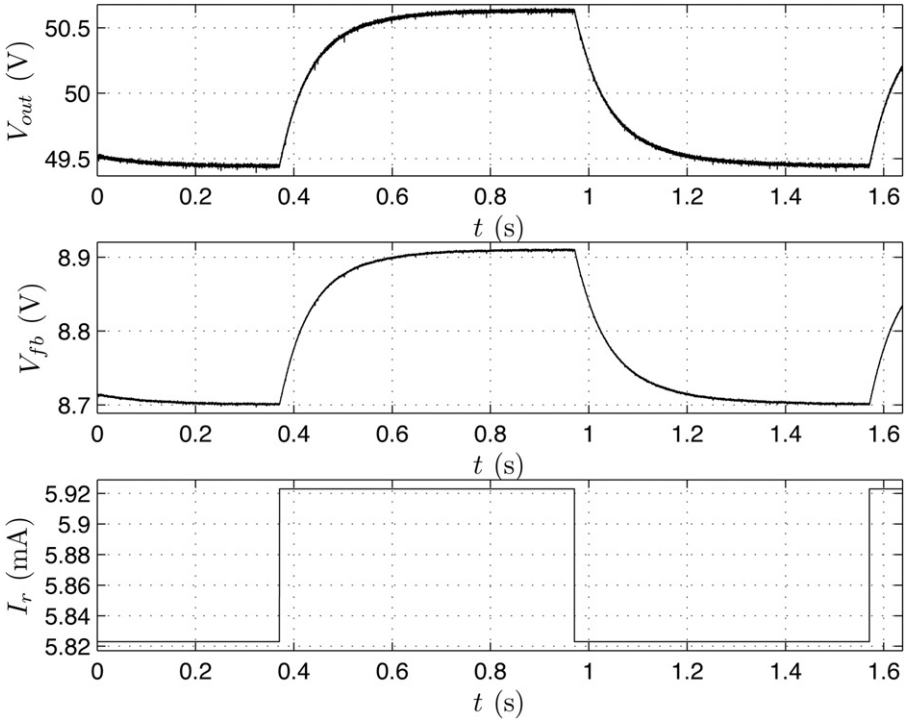


**Fig. 17.** Transient responses of the boost converter supplied by the fuel cell emulator (output voltage $V_{out}$ and feedback voltage $V_{fb}$) on the change of control signal $I_r(t)$, with $I_{out}$ = 1 A, $V_{in} = V_{FC}$ = 28 V.

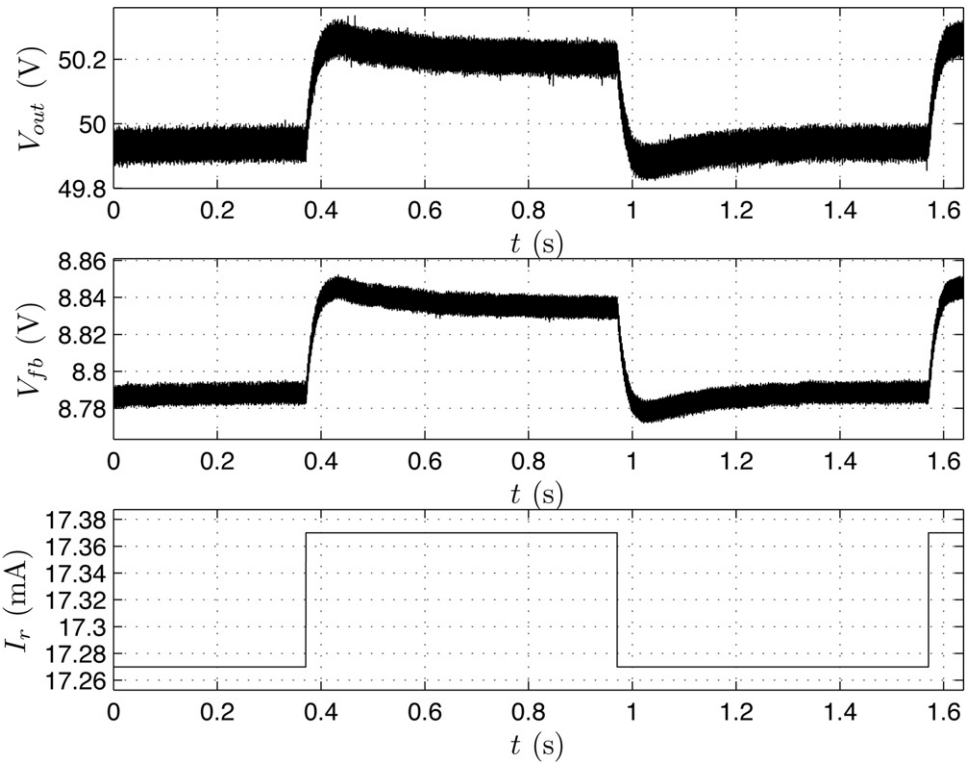


**Fig. 18.** Transient responses of the boost converter supplied by the fuel cell emulator (output voltage $V_{out}$ and feedback voltage $V_{fb}$) on the change of control signal $I_r(t)$, with $I_{out} = 9$ A, $V_{in} = V_{FC} = 20.5$ V.

$I_{out} = 1$ A, and $G_9$ for the last (boundary) operating point determined by $I_{out} = 9$ A, with included feedback element (89):

$$G_1(s) = \frac{\Delta v_{fb}(s)}{\Delta i_r(s)} = \frac{2088 \cdot (1 + 0.0186s)}{(1 + 0.0745s)(1 + 0.016s)(1 + 0.00035s)},$$
$$G_9(s) = \frac{\Delta v_{fb}(s)}{\Delta i_r(s)} = \frac{461 \cdot (1 + 0.1576s)}{(1 + 0.1142s)(1 + 0.0171s)(1 + 0.00035s)}. \quad (93)$$

Figs. 19 and 20 show that the maximum errors of linearized models are dominantly determined by the standard deviation of the output voltage ripple and noise, so the derived transfer functions (87) accurately describe the behavior of the DC/DC boost converter supplied by the fuel cell emulator.

The obtained results for all operating points are summarized in Table 2. Additionally, the Bodé plot of the frequency characteristics of the obtained model (87), with parameters given in Table 2, are shown in Fig. 21.

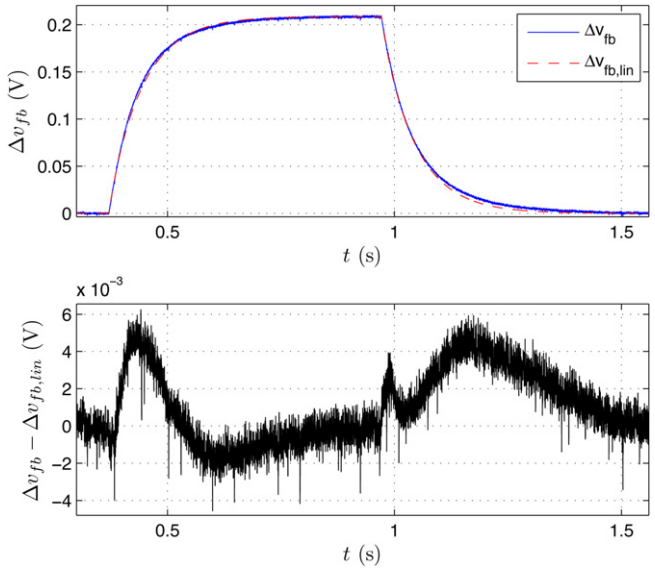


**Fig. 19.** The recorded transient of converter output voltage without initial value and the transient response of the model $G_1$ (93) on the change of control signal $I_r(t) = 5.823 + 0.1\mathrm{S}(t - 0.37) - 0.1\mathrm{S}(t - 0.97)$ mA, with conditions according to Fig. 17 caption.

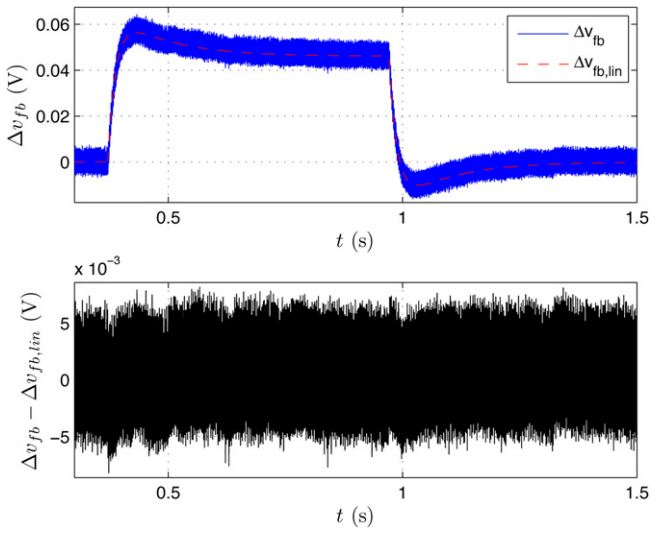


**Fig. 20.** The recorded transient of converter output voltage without initial value and the transient response of the model $G_9$ (93) on the change of control signal $I_r(t) = 17.27 + 0.1\mathrm{S}(t - 0.37) - 0.1\mathrm{S}(t - 0.97)$ mA, with conditions according to Fig. 18 caption.

**Table 2**
The parameters of the linear model (87) of the boost converter supplied by the fuel cell emulator $K$, $T_b$, $T_1$ and $T_2$ obtained in several operating points determined by the output current $I_{out}$.

| $I_{out}$ (A) | $V_{in}$ (V) | $K$ | $T_b$ (ms) | $T_1$ (ms) | $T_2$ (ms) |
|---|---|---|---|---|---|
| 1 | 28.0 | 2088 | 18.6 | 16.0 | 74.5 |
| 3 | 24.7 | 1556 | 33.8 | 31.7 | 22.7 |
| 5 | 23.5 | 734.6 | 94.7 | 84.1 | 19.5 |
| 7 | 22.2 | 595.0 | 122.4 | 102.0 | 18.3 |
| 9 | 20.5 | 461.0 | 157.6 | 114.2 | 17.1 |

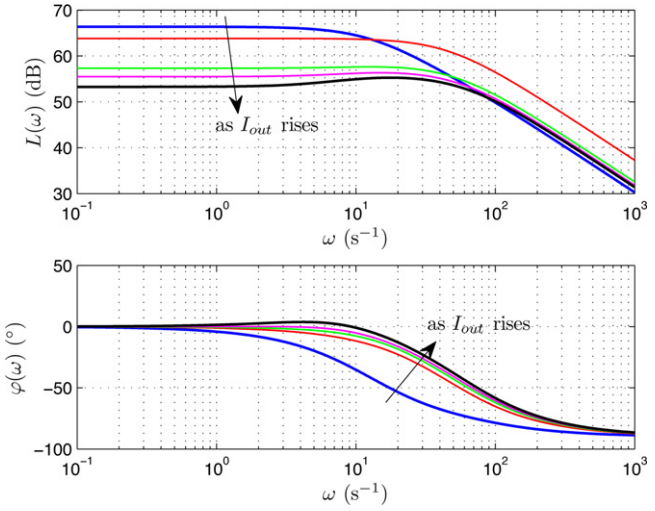


**Fig. 21.** The Bodé plot of the frequency characteristics of the obtained model (87), with parameters given in Table 2.

The transient responses in other operating points, given in Table 2, are similar to the responses in the described boundary operating points, which means that maximum error of the linear model is also determined by the standard deviation of the output voltage ripple and noise. In explanation, the transfer functions (87), along with the appropriate parameters from Table 2, accurately describe the behavior of the peak current mode DC/DC boost converter in the given operating point determined by the output current.

## 6. Conclusion

The linear model of the constant frequency peak current mode controlled DC/DC boost converter supplied by the PEM fuel cell stack is derived in this paper. The parameters of the linear model vary with the operating point, determined by the load resistance or output current. The contribution of the paper is in deriving the transfer function of boost converter output voltage with respect to the control (referent) current of the converter, with included compensation ramp in the continuous and especially in the discontinuous conduction mode. Even though it is not necessary for the stabilization of the system in the discontinuous conduction mode, it is hard to turn off the compensation ramp when transferring from the continuous to the discontinuous conduction mode and vise versa, so it must be included in the discontinuous conduction mode as well. The model is valid in the whole range of converter and fuel cell normal operating conditions, which makes it suitable for advanced controller design, which will result in approximately the same dynamic behavior of the system irrespective of the operating point and/or conduction mode. The parameters of the model are obtained experimentally in two boundary operating points that represent minimal and nominal load power consumption, and in three other between the boundary operating points. The linear model errors are determined by the standard deviation of the output voltage ripple and noise, so the derived model with appropriate parameters accurately describes the system in the given operating point.

## Acknowledgements

This work has been funded by the Ministry of Science, Education and Sports of the Republic of Croatia.

The authors would like to thank the Croatian company Mareton Power Electronics for the design and making of the special version of the boost converter, which enabled the experimental verification of the obtained model.

## References

[1] J.M. Andújar, F. Segura, M.J. Vasallo, Renewable Energy 33 (4) (2008) 813–826.
[2] W. Choi, J.W. Howze, P. Enjeti, Journal of Power Sources 157 (1) (2006) 311–317.
[3] R. Dufo-López, J.L. Bernal-Agustín, J. Contreras, Renewable Energy 32 (7) (2007) 1102–1126.
[4] K. Jin, X. Ruan, M. Yang, M. Xu, IEEE Transactions on Industrial Electronics 56 (4) (2009) 1212–1222.
[5] A. Kirubakaran, S. Jain, R.K. Nema, Renewable and Sustainable Energy Reviews 13 (9) (2009) 2430–2440.
[6] V. Paladini, T. Donateo, A. de Risi, D. Laforgia, Energy Conversion and Management 48 (11) (2007) 3001–3008.
[7] F. Segura, E. Durán, J.M. Andújar, Journal of Power Sources 193 (1) (2009) 276–284.
[8] P. Thounthong, B. Davat, Energy Conversion and Management 51 (4) (2010) 826–832.
[9] P. Thounthong, S. Raël, IEEE Industrial Electronics Magazine 3 (3) (2009) 25–37.
[10] P. Thounthong, P. Sethakul, S. Rael, B. Davat, in: IEEE International Conference on Industrial Technology, 2009 (ICIT 2009), 10–13 February 2009, Gippsland, Vic., pp. 1–6, ISBN: 978-1-4244-3506-7, doi:10.1109/ICIT.2009.4939566.
[11] M. Uzunoglu, O.C. Onar, M.S. Alam, Renewable Energy 34 (3) (2009) 509–520.
[12] Y. Yang, Z. Liu, F. Wang, Journal of Power Sources 179 (2) (2008) 618–630.
[13] T. Bjažić, Ž. Ban, I. Volarić, International Symposium on Industrial Electronics – ISIE2008, 2008.
[14] Y. Kim, Journal of Power Sources 195 (19) (2010) 6329–6341.
[15] G. Ji, F. Chen, T. Ma, C. Zhang, Y. Zhou, S. Zhou, in: IEEE International Conference on Control and Automation, 2009 (ICCA 2009), 9–11 December 2009, Christchurch, pp. 2100–2105, ISBN: 978-1-4244-4706-0, doi:10.1109/ICCA.2009.5410353.
[16] J. Jia, S. Yang, Y. Wang, Y.T. Cham, in: IEEE International Conference on Control and Automation, 2009 (ICCA 2009), 9–11 December 2009, Christchurch, pp. 1657–1662, ISBN: 978-1-4244-4706-0, doi:10.1109/ICCA.2009.5410529.
[17] F. Khorrami, S. Puranik, A. Keyhani, P. Krishnamurthy, Y. She, in: Proceedings of the 48th IEEE Conference on Decision and Control, 2009 held jointly with the 28th Chinese Control Conference (CDC/CCC 2009), 15–18 December 2009, Shanghai, pp. 7860–7865, ISBN: 978-1-4244-3871-6, doi:10.1109/CDC.2009.5400280.
[18] E. Kim, C. Kim, in: International Conference on Electrical Machines and Systems, 2009 (ICEMS 2009), 15–18 November 2009, Tokyo, pp. 1–5, ISBN: 978-1-4244-5177-7, doi:10.1109/ICEMS.2009.5382682.
[19] E. Kim, C. Kim, in: 31st International Telecommunications Energy Conference, 2009 (INTELEC 2009), 18–22 October 2009, Incheon, pp. 1–3, ISBN: 978-1-4244-2490-0, doi:10.1109/INTLEC.2009.5351946.
[20] J. Li, L. Xu, J. Hua, M. Ouyang, in: ASME 2009 7th International Conference on Fuel Cell Science, Engineering and Technology (FUELCELL2009), 8–10 June 2009, Newport Beach, California, USA, pp. 501–507, ISBN: 978-0-7918-4881-4, doi:10.1115/FuelCell2009-85203.
[21] K. Mammar, A. Chaker, Journal of Electrical Engineering 60 (6) (2009) 328–334.
[22] *, BCS Fuel Cell Model 64-32 – Operating Manual, BCS Fuel Cells, Inc., 2006.
[23] M. Milanovič, Močnostna Elektronika, Fakulteta za elektrotehniko i računalništvo in informatiko, Maribor, 2007.
[24] R.B. Ridley, in: 21st Annual IEEE Power Electronics Specialists Conference, 1990 (PESC '90 Record.), 11–14 June 1990, San Antonio, TX , USA, pp. 382–389, doi:10.1109/PESC.1990.131213.
[25] R.B. Ridley, IEEE Transactions on Power Electronics 6 (2) (1991) 271–280.
[26] J. Kassakian, M. Schlecht, G. Verghese, Principles of Power Electronics, Addison-Wesley Publishing Company, Reading, MA, 1992.
[27] J. Sun, D.M. Mitchell, M.F. Greuel, P.T. Krein, R.M. Bass, IEEE Transactions on Power Electronics 16 (4) (2001) 482–492.
[28] T. Suntio, M. Hankaniemi, T. Roinila, Simulation Modelling Practice and Theory 15 (10) (2007) 1320–1337.
[29] J. Alvarez-Ramirez, G. Espinosa-Pérez, Systems and Control Letters 45 (2) (2002) 113–119.

[30] T. Bjažić, Adaptive control of the DC/DC boost converter supplied by the fuel cell, Ph.D. Thesis, University of Zagreb, Faculty of Electrical Engineering and Computing, 2010.
[31] J.M. Corrêa, F.A. Farret, L.N. Canha, M.G. Simoes, IEEE Transactions on Industrial Electronics 51 (5) (2004) 1103–1112.
[32] F. Barbir, PEM Fuel Cells: Theory and Practice, Elsevier Academic Press, 2005.
[33] R.F. Mann, J.C. Amphlett, M.A.I. Hooper, H.M. Jensen, B.A. Peppley, P.R. Roberge, Journal of Power Sources 86 (1) (2000) 173–180.
[34] T. Bjažić, Ž. Ban, M. Perković Franjić, Proceedings of the 30th Jubilee International Convention on Information and Communication Technology, Electronics and Microelectronics: Computers in Technical Systems, Opatija, 2007, pp. 46–51.
[35] C. Kunusch, A. Husar, P.F. Puleston, M.A. Mayosky, J.J. Moré, International Journal of Hydrogen Energy 33 (13) (2008) 3581–3587.
[36] T. Bjažić, Ž. Ban, Proceedings of the 31st International Convention on Information and Communication Technology, Electronics and Microelectronics: Computers in Technical Systems, 2008.
[37] Y. Zhang, M. Ouyang, Q. Lu, J. Luo, X. Li, Applied Thermal Engineering 24 (2004) 501–513.
[38] N. Perić, M. Jelavić, Ž. Ban, H. Domitrović, B. Matijašević, M. Kostelac, S. Mikac, in: 2010 European Wind Energy Conference & Exhibition (EWEC 2010), http://www.ewec2010proceedings.info/proceedings/index2test.php.
[39] *, 600 W Electronic Load Module: Agilent Model 60504B – Operating Manual, Agilent Technologies, 1991.
[40] *, Electronic Load Mainframes: Models 6050A and 6051A – Operating Manual, Agilent Technologies, 2000.
[41] *, CompactRIO Developers Guide, National Instruments, 2009.
[42] *, LabVIEW FPGA, National Instruments, 2009.